

RESEARCH ARTICLE

3D Printing of a Graphene-Modified Photopolymer Using Stereolithography for Biomedical Applications: A Study of the Polymerization Reaction

S. Lopez de Armentia^{1*}, S. Fernández-Villamarín¹, Y. Ballesteros¹, J. C. del Real¹,
N. Dunne^{2,3,4,5,6,7,8,9}, E. Paz^{1*}

¹Department of Mechanical Engineering, Institute for Research in Technology, Universidad Pontificia Comillas, Alberto Aguilera 25, 28015 Madrid, Spain

²School of Mechanical and Manufacturing Engineering, Dublin City University, Dublin 9, Ireland

³Centre for Medical Engineering Research, School of Mechanical and Manufacturing Engineering, Dublin City University, Dublin 9, Ireland

⁴School of Pharmacy, Queen's University of Belfast, 97 Lisburn Road, Belfast BT9 7BL, United Kingdom

⁵Department of Mechanical and Manufacturing Engineering, School of Engineering, Trinity College Dublin, Dublin 2, Ireland

⁶Advanced Manufacturing Research Centre (I-Form), School of Mechanical and Manufacturing Engineering, Dublin City University, Glasnevin, Dublin 9, Ireland

⁷Advanced Materials and Bioengineering Research Centre (AMBER), Royal College of Surgeons in Ireland and Trinity College Dublin, Dublin 2, Ireland

⁸Advanced Processing Technology Research Centre, Dublin City University, Dublin 9, Ireland

⁹Trinity Centre for Biomedical Engineering, Trinity Biomedical Sciences Institute, Trinity College Dublin, Dublin 2, Ireland

Abstract: Additive manufacturing is gaining importance thanks to its multiple advantages. Stereolithography (SLA) shows the highest accuracy and the lowest anisotropy, which has facilitated the emergence of new applications as dentistry or tissue engineering. However, the availability of commercial photopolymers is still limited, and there is an increasing interest in developing resins with properties adapted for these new applications. The addition of graphene-based nanomaterials (GBN) may provide interesting advantages, such as improved mechanical properties and bioactivity. However, there is a lack of knowledge regarding the effect of GBNs on the polymerization reaction. A photopolymerizable acrylic resin has been used, and the effect of the addition of 0.1 wt% of graphene (G); graphene oxide (GO) and graphite nanoplatelets (GoxNP) on printability and polymerization have been investigated. It was observed that the effect depended on GBN type, functionalization and structure (e.g., number of layers, size, and morphology) due to differences in the extent of dispersion and light absorbance. The obtained results showed that GO and GoxNP did not significantly affect the printability and quality of the final structure, whilst the application of G exhibited a negative effect in terms of printability due to a reduction in the polymerization degree. GO and GoxNP-loaded resins showed a great potential to be used for manufacturing structures by SLA.

Keywords: Nanocomposites; Graphene-based nanomaterials; Stereolithography; Photocurable polymer; Printing accuracy

*Correspondence to: S. Lopez de Armentia, Department of Mechanical Engineering, Institute for Research in Technology, Universidad Pontificia Comillas, Alberto Aguilera Madrid, Spain; sara.lopez@comillas.edu; E. Paz, Department of Mechanical Engineering, Institute for Research in Technology, Universidad Pontificia Comillas, Alberto Aguilera 25, 28015 Madrid, Spain; eva.paz@comillas.edu

Received: September 20, 2021; **Accepted:** December 19, 2021; **Published Online:** January 13, 2022

Citation: Lopez de Armentia S, Fernández-Villamarín S, Ballesteros Y, *et al.*, 2022, 3D Printing of a Graphene-Modified Photopolymer Using Stereolithography for Biomedical Applications: A Study of the Polymerization Reaction. *Int J Bioprint*, 8(1):503. <http://doi.org/10.18063/ijb.v8i1.503>

© 2022 Author(s). This is an Open Access article distributed under the terms of the Creative Commons Attribution License, permitting distribution and reproduction in any medium, provided the original work is properly cited.

1. Introduction

Additive manufacturing (AM) is a promising and versatile technology for the fabrication of customized structures in terms of design. Since its invention in the late 1980s, different types of 3D printers have been developed. Printers based on vat photopolymerizations (stereolithography [SLA] and digital light projection [DLP]) were the first commercially available printers^[1]. The difference between SLA and DLP relates primarily to the light source. SLA technology uses a light from a single laser beam of ultraviolet (UV) light, that forms the layer point-by-point by changing the orientation of optical elements such as mirrors or lenses. However, in the case of DLP printers, the entire layer is cured at the same time using an array of mirrors that project UV light to the pattern of the printed cross-section^[2].

In particular, the biomedical engineering field needs to have the ability to fabricate customized structures at relatively low-volume levels. Therefore, AM is ideal for such applications. Furthermore, AM offers the potential for accurate control of geometry and dimensions, which is vital for the biomedical engineering field. Among the different technologies, SLA offers some advantages: (i) it presents the highest accuracy, (ii) SLA-created structures can have smooth surfaces, and (iii) the materials used in SLA technology can be easily sterilized by UV. At present, SLA is already used in biomedical engineering applications, such as in dentistry^[3,4], soft tissue-engineering^[5,6], hard tissue-engineering^[7,8], delivery device fabrication^[9,10], and biopharmaceutical manufacture^[11,12].

Recently, there is an increasing interest in the improvement of commercially available photocurable resins to modify the electrical^[13-17], mechanical^[15,18-21], biological^[22], and/or polymerization^[23] properties and adapt these properties toward emerging biomedical engineering applications. A promising way to modify and tailor the properties of the photocurable resin could be through the dispersion of nanomaterials within the resin.

One of the most interesting nanomaterials that is currently receiving significant research attention is graphene (G), which demonstrates high surface area, superior mechanical properties, thermal and electrical conductivity, excellent intrinsic carrier mobility, and barrier properties among other interesting qualities^[24,25]. The main limitation of G is its difficulty to be manufactured at scale and its tendency to form agglomerates when being dispersed within a solution^[26]. In general, other G-based nanomaterials, such as graphene oxide (GO) or graphite nanoplatelets (GoxNP), present lower properties than G (in terms of mechanical or electrical properties), but they demonstrate the ability to be manufactured at scale and they present better dispersibility.

To achieve the advantages that nanomaterials offer, it is important to obtain a good dispersion within the matrix materials. Many methods have been investigated to improve the graphene-based nanomaterials (GBN) dispersion within the matrix materials and reduce the incidence of agglomerate formation. To achieve a good dispersion, it is important to pay particular attention to the methods used for stirring and dispersion, and also chemical functionalization of the GBN.

In terms of stirring and dispersion, techniques such as sonication using a soniprobe^[27,28] or bath^[29], high-shear mixing^[30], high-speed disk^[31], and calendaring processes^[32,33] have been commonly applied. When the resin viscosity is too high, then ultrasonic or mechanical mixing cannot be applied successfully; therefore, it is necessary to reduce the resin viscosity. For this purpose, different solvents have been used, for example, THF^[28], acetone^[27,34], isopropanol^[29], and water^[35]. To improve GBN dispersion, chemical functionalization such as polymer grafting^[28], self-assembly functionalization^[34], and the use of dispersants^[35,36] have also successfully applied.

At present, GBN has been introduced to AM technology with respect to the fabrication of SLA printed constructs. In terms of biomedical engineering applications, GBN have been reported to offer enhanced mechanical properties^[21,37-39], promote cell differentiation^[22], and increase hydrophilicity and subsequently improve cell adhesion^[40].

However, with respect to SLA and DLP techniques, there is currently a lack of knowledge about the influence of GBNs on the polymerization reaction, but some issues relating to delamination^[41] and a reduction in maximum curable thickness per scan^[42] have been reported when GBNs were incorporated into photocurable resins. With the addition of nanomaterials into the resin, a competition takes place in terms of light absorption between the photoinitiator and nanomaterial. Usually, this competition leads to a less effective UV polymerization process.

Nanomaterials may influence the UV polymerization reaction due to changes in optical properties, which results in variations in absorbance or transmittance of the resin^[17,19]. They also can act as light scattering and shielding center^[43]. Besides, the polymerization reaction may be affected by the nanomaterial^[44,45] if they act as chain transfer agent, thereby inhibiting polymer chain growth^[39], or as free radical scavengers that reduce the extent of polymerization reaction^[46,47]. These effects make studying the influence of nanomaterials especially important, specifically their effect on the polymerization reaction of photocurable resins and in the context of efficacious 3D printing, as these modifications can affect printability and the practicality of a particular 3D printing technique. These effect depends on many factors, for

example, type and specific surface area of the nanomaterial – the latter factor affects the extents of shielding, which can affect the degree of polymerization^[48].

In this study, the effect of incorporating a particular GBN (G, GO and GoxNP) into a commercial photosensitive resin has been investigated. Specifically, the thermal properties and the polymerization reaction were investigated using Fourier transform infrared (FTIR) spectroscopy and differential scanning calorimetry (DSC). The influence of GBN incorporation into the polymer resin was also determined in terms of rheological, physicochemical and surface properties, as well as dimensional accuracy and printability following 3D printing.

2. Materials

The photocurable acrylic-based resin was Formlabs Clear FLGPCL4 (Formlabs, MA, USA). The GBN used were: (i) G supplied by Avanzare Nanotechnology (La Rioja, Spain), (ii) GO and (iii) GoxNP, which were both supplied by NanoInnova Technologies (Toledo, Spain). According to materials data sheet, G was composed of 1 – 2 sheets of 2 – 4 μm of average lateral size and 0.7 nm of thickness. GO demonstrated an average lateral sheet of 4 – 8 μm and a thickness of 0.7 – 1.2 nm, while the GoxNP was composed of less than five layers and an average size of 2 – 3 μm . The oxygen content of GoxNP was approximately 2%.

Scanning electron microscope (SEM) images of the different GBN (**Figure 1**) were taken by TENEEO-LoVac (Eindhoven, the Netherlands). The lateral size of the different GBN given by the manufacturer in the datasheet corresponded to the size measured by SEM.

3. Experimental methodology

3.1. Specimen preparation

Polymer resin blends containing 0.1 wt% of each GBN were prepared and homogeneously mixed to ensure the full dispersion of the nanomaterial. The wt% of nanomaterial used was based on a previous study^[49], which reported that 0.1 wt% of G and GO demonstrated significant improvement in mechanical performance when incorporated into an acrylic-based resin for orthopedic applications.

Initially, the nanofiller (i.e., G, GO or GoxNP) was homogenized in the polymer resin through sonication using a digital sonifier (Branson 450, Branson Ultrasonics Corp., CT, USA). Specifically, the frequency range applied was 1,985–2,050 kHz at a 30% amplitude for 30 ± 0.5 min – pulses of 10 ± 0.5 s on and 20 ± 0.5 s off were applied, and the solution was placed in an ice bath ($6 \pm 2^\circ\text{C}$) to avoid overheating. Finally, degasification was undertaken in a vacuum drying oven (Vaciotem-T,

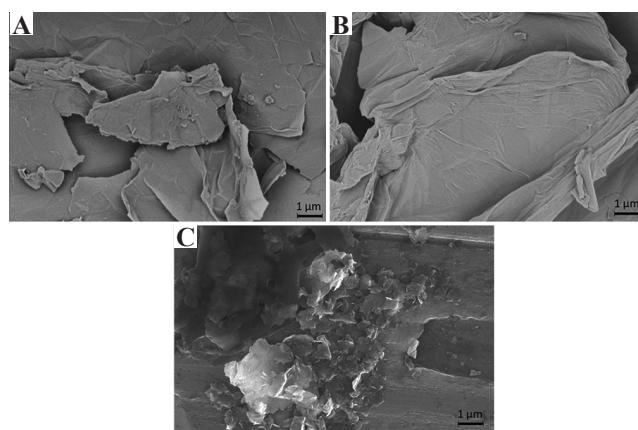


Figure 1. Scanning electron microscope images of the different graphene-based nanomaterials. (A) Graphene. (B) Graphene oxide. (C) Graphite nanoplatelets.

Selecta, Spain) 15 ± 0.5 min followed by placement in and ultrasonic bath (Elmasonic p60h, Elma Schmidbauer GmbH, Germany) for 15 ± 0.5 min.

3.2. Viscosity

The viscosity was measured at 31°C , the printing temperature, using a rotational viscometer Fungilab Smart Serie (Fungilab, Barcelona, Spain). The measurements were made using a R3 stainless steel spindle at a rotation speed of 100 RPM. At least three measurements were conducted for each sample.

3.3. DSC

The extent of the polymerization reaction of the resin and the effect of nanofiller incorporation was determined using DSC, which was measured using DSC 882e Mettler Toledo (Greifensee, Switzerland). The Formlabs Clear resin can cure through two different mechanisms (or a combination of both): (i) Thermal polymerization – by the application of temperature and (ii) UV polymerization – by the application of UV light at 405 nm wavelength. To determine the effect of nanofiller incorporation on these mechanisms, two different DSC tests were performed: (i) Complete thermal polymerization energy of the samples was determined (without UV polymerization), and (ii) degree of UV polymerization was studied by subjecting the sample to different exposure times and completing the cure by thermal energy.

(I) Thermal polymerization

Thermal polymerization of pristine (R) and reinforced (R+G, R+GO and R+GoxNP) resin was studied with a heating ramp from 20°C to 250°C at $10^\circ\text{C}/\text{min}$. Three tests of each sample were performed and the DSC thermogram of heat flow versus polymerization time was obtained. From these tests, the effect of nanofillers on

thermal polymerization energy (E_{total}) and polymerization temperature was studied. The E_{total} expressed in J/g was determined as the area under the heat flow versus polymerization time curve.

(2) UV polymerization

To study the UV polymerization process and the effect that nanofillers could have on the UV polymerization degree, three samples of the pristine and the reinforced resin were cured inside a Form Cure chamber (Formlabs, Somerville, MA, USA), during different exposure times. The wavelength used for the UV cure was 405 nm, the same value during the printing of the samples. After UV exposition, DSC analysis was carried out to the samples with a heating ramp from 20°C to 250°C at 10°C/min to complete the cure of the samples. By knowing the E_{total} and the energy needed to complete polymerization after UV (E_{tc}), polymerization degree due to UV radiation may be calculated (Eq. 3.1).

$$\text{Curing degree}(\%) = \frac{E_{total} - E_{tc}}{E_{total}} \times 100 \quad (3.1)$$

(3) Glass transition temperature

The glass transition temperature (T_g) of each 3D printed sample was also determined. The heating ramp used in this case was from 20 to 200°C with a heating rate of 20°C/min. T_g was measured using the midpoint value. All DSC tests were conducted using aluminum crucibles with a capacity of 40 μ L and 50 μ m hole in the lid; the amount of sample tested was between 10 and 15 mg. Nitrogen was used as the purging gas and was delivered at a rate of 80 mL/min.

3.4. Fourier-transformed infrared spectroscopy

Infrared spectra were obtained with a Tensor27 FTIR spectrometer from Bruker (Bruker Optik GmbH, Madrid, Spain), with attenuated total reflectance (ATR) technique. Golden Gate ATR accessory (Specac, Orpington, UK) formed by a 0.5 mm diameter diamond embedded in a ZnSe crystal was used. The ratio signal-to-noise is better than 8000:1 (5.4×10^{-5} noise absorbance). Spectra were recorded with a resolution of 4 cm^{-1} from 4000 to 400 cm^{-1} across 32 scans.

FTIR spectra at different UV polymerization times, prepared as previously explained, were normalized from the peak of $-\text{CH}_3$ symmetric stretching (1375 cm^{-1}), and the polymerization process was followed by observing the reduction of the C=C peak (1,636 cm^{-1})^[50].

3.5. Hardness

Furthermore, Shore D hardness was measured for 3D printed samples as a function of different UV exposure

times. Shore D hardness tester (Bareiss GmbH, Berlin, Germany) was used for these measurements, applying 50 N, following the standard UNE-EN ISO 868. At least four measurements were taken for each sample.

3.6. UV-visible spectroscopy

Absorbance of the different samples at wavelength of 405 nm was measured by UV-visible spectroscopy using a Cary 4000 UV-visible spectrophotometer (Agilent Technologies, Santa Clara, CA, USA). R sample was used as reference to study the absorbance of the nanofillers.

3.7. Printability and dimensional stability

The effect of the nanofillers on printability and dimensional stability was studied by 3D printing cube samples containing holes of different geometric shapes (i.e., circular and square holes) on their faces in order to determine if the addition of nanoparticles influences the quality and accuracy of the 3D printed samples. To obtain micrographs, an Olympus DSX1000 digital microscope (Olympus, Shinjuku, Tokyo, Japan) was used. Image measurement was completed with GIMP 2.10.12 software. The background of the image was removed, and it was transformed into a binary image. The difference image with the reference (CAD file) was obtained and black and white pixels were counted. Accuracy was obtained using Eq. 3.2^[51]:

$$\% \text{Accuracy} = \frac{\text{Black pixels}}{\text{Black pixels} + \text{White pixels}} \times 100 \quad (3.2)$$

3.8. Dispersibility

Dispersibility of the GBN was observed by opto-digital microscopy on printed samples surface. Olympus DSX1000 (Olympus, Shinjuku, Tokyo, Japan) was used with polarized light to observe GBN agglomerates.

3.9. Thermal conductivity

Thermal conductivity was measured using DSC following the procedure proposed by Hakvoort and van Reijen^[52] As pure metal, gallium, was used and silicone oil was applied to improve the contact with the sample, which was cut into cylinders with a height between 1 and 2 mm, and a diameter of 6 mm. The scan was set from 28 to 38°C at 0.5°C/min. At least 5 measurements were completed for each sample and outliers were detected by Grubbs test with $\alpha = 0.01$.

3.10. Wettability

Cell adhesion is influenced by surface hydrophilicity,^[53] and an improvement in this parameter could improve

the potential application in biomedical field. Besides, wettability measurements can give information about layers adhesion since polymerized layer has to be wetted by liquid resin to obtain adequate adhesion between the polymerized layer and the new one.

Hydrophilicity was studied by measuring the contact angle of water on the sample surface at room temperature (20°C). Dataphysics OCA15 plus goniometer and SCA20 software (DataPhysics Instruments GmbH, Filderstadt, Germany) were used for this purpose. At least ten contact angles were measured for each sample.

3.11. Surface roughness

Surface roughness of each 3D printed sample was measured using optical microscopy. Specifically, Olympus DSX1000 was used with $\times 10$ zoom and bright field. 3D images were captured and from these images, at least six line-measurements at random directions were completed for each sample and the roughness parameters were obtained using the Software Olympus Stream (Olympus, Shinjuku, Tokyo, Japan).

3.12. Statistical analysis

The results were also evaluated for statistical significance using a one-way analysis of variance (ANOVA) test with a *post hoc* Scheffe's test (SPSS 20.0 for Windows; IBM SPSS, USA). A $P < 0.05$ was indicative of statistical significance.

4. Results

4.1. Viscosity

It is observed that in comparison with R, the incorporation of G produced a marked decrease of the viscosity (59.1%); on the contrary, the incorporation of GO and GoxNP showed a slight increase by 18.2 and 25%, respectively (Table 1). These differences are not statistically significant; however, significant differences were found between R+G viscosity and R+GO/R+GoxNP viscosity.

The reduction of viscosity could be due to an increase in free volume generated around the nanoparticles^[54]. To corroborate this hypothesis, T_g measurements were

Table 1. Viscosity of R, R+G, R+GO, R+GoxNP

Material Type	Viscosity at 31°C (Pa·s)	T_g (°C)
R	$0.44 \pm 0.02^{a,b}$	106 ± 3
R+G	0.18 ± 0.09^a	73 ± 4
R+GO	0.52 ± 0.07^b	105 ± 2
R+GoxNP	0.55 ± 0.06^b	108 ± 3

Viscosity is expressed as mean \pm standard deviation. Values with different letters are significantly different ($P < 0.05$). When a statistical analysis is carried out, different P -values were obtained for each pair of data giving information about the significance of the differences. Superscript letters a and b are used to identify which pairs of values are significantly different.

completed. It was observed that the addition of G significantly reduced the T_g value, from 106°C to 73°C. However, GO and GoxNP showed similar T_g than R (Table 1).

4.2. Thermal polymerization

It can be noted that the required energy (E_{total}), calculated by measuring the area under the polymerization peak (Figure 2), is similar for all material formulations investigated, all the values are in the range from 21.2 to 22 J/g. Peak temperatures (polymerization temperatures) are between 179 and 185°C, the values are also similar for all resins (Table 2).

4.3. UV polymerization

The effect of applying different polymerization times during polymerization was compared. As example, pristine resin DSC curves are shown in Figure 3. It can be observed that when samples are irradiated with UV light, DSC curves show two exothermic peaks; the first one was between 70 and 84°C and the second one between 146 and 166°C, depending on the UV exposure time. To the best of our knowledge, there were no similar studies using photocurable polymers; however, Vicard *et al.*^[55] have reported DSC curves of polymerization-crystallization process of polyamides. They reported a first exothermic peak of polymerization, followed by another exothermic peak that corresponds to the crystallization of the polymer formed in the previous peak.

In this study, there was some cured polymer from the beginning of the test due to the UV exposition. Therefore, the first peak could be assigned to the crystallization or crosslinking of the UV cured polymer (UV-peak), whilst the second peak could be due to the thermal polymerization of the non-UV polymerized resin (thermal-peak).

For all material types investigated, the same trend was observed in relation with these two exothermic

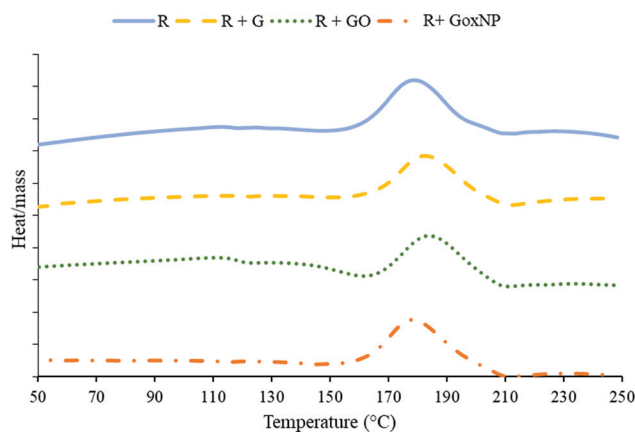


Figure 2. Differential scanning calorimetry thermograms of R, R+G, R+GO, R+GoxNP.

peaks and the increase in the UV exposure time. The first peak increases with UV time due to the increment of cured polymer by photopolymerization – the greater the UV-cured polymer, the greater the necessary energy to crosslink it when temperature was applied. In contrast, as expected, the peak of the thermal polymerization decreased as a function of UV time – the greater the UV-cured polymer, the lower the remaining uncured polymer. When it is exposed to UV radiation for 30 min, UV-polymerization of the resin will be completed and therefore, the peak of thermal polymerization disappears.

Table 3 summarizes DSC energies obtained from DSC thermograms for each measured time and each nanofiller. It can be observed that at 0 min, all the samples showed similar behavior – non-UV-peak and a similar thermal peak with an energy of about 21 – 22 J/g. However, for low UV exposure times (1 min), when the nanocomposites are compared to R, it was observed that all nanofillers reduced the extent of UV polymerization, with E_{UV} lower than 3 J/g whilst R reached 11.3 J/g. From 5 min, this reduction was only found on the addition of G and GoxNP, being the energies of R+GO similar than R. Finally, for longer times (20 min), R+G was the only material type that showed differences compared to R.

FTIR spectrum of uncured resin is shown in **Figure 4**. Peaks corresponding to an acrylic resin are observed in the spectra. Alkyl groups are found as two peaks in the range of 2870 – 2950 cm^{-1} [56], whilst the bonds C=O, C-O and -C-C(=O)-O- of ester group appear at 1707, 1636 and 1165 cm^{-1} , respectively[57].

Using FTIR analysis, the polymerization process can be followed as the polymerization occurs by the opening of C=C bond at 1637 cm^{-1} [50]. The detail of the

Table 2. Polymerization energy and polymerization temperature of R, R+G, R+GO, R+GoxNP

Material type	Polymerization energy ($\text{J}\cdot\text{g}^{-1}$)	Polymerization temperature ($^{\circ}\text{C}$)
R	22.0 ± 2.3	179 ± 3
R+G	21.6 ± 1.8	183 ± 2
R+GO	21.2 ± 1.6	185 ± 4
R+GoxNP	21.6 ± 2.2	179 ± 3

Polymerization energy and polymerization temperature is expressed as mean \pm standard deviation.

Table 3. Mean DSC energies ($\text{J}\cdot\text{g}^{-1}$) of R, R+G, R+GO, R+GoxNP

Min	R		R+G		R+GO		R+GoxNP	
	E_{UV}	E_{tc}	E_{UV}	E_{tc}	E_{UV}	E_{tc}	E_{UV}	E_{tc}
0	0.0	22.0	0.0	21.6	0.0	21.2	0.0	21.6
1	11.3	15.9	1.3	23.4	2.8	22.2	2.2	24.3
5	18.1	1.5	13.2	9.7	17.5	2.3	11.9	9.6
10	18.3	1.5	15.8	4.8	18.0	2.1	18.6	4.0
20	22.9	0.7	17.9	2.8	19.7	0.0	21.0	1.1

decreasing of this peak with the UV exposure time is shown in **Figure 5**. It can be seen how it decreases as the UV polymerization time increases, until its disappearance at 30 min, when the polymer is completely cured. This complete polymerization time is in accordance with the DSC results previously discussed.

To determine the effect of nanofillers addition on the UV polymerization process, DSC and FTIR results were compared for all samples at the same UV exposure time. **Figure 6** shows the effect of the different nanofillers for 5 min of polymerization on the DSC thermograms. The first peak, located between 70 and 80 $^{\circ}\text{C}$, as commented above, was due to the crystallization of the polymer cured by UV. The higher was the UV polymerization degree, the greater was this crystallization peak. It can be seen how G and GoxNP presence reduced the area of this peak, suggesting that for the same UV exposure time, the UV polymerization degree was lower in the case of these nanofillers.

The second peak (150 – 160 $^{\circ}\text{C}$) corresponded to the thermal polymerization process of the uncured polymer. Obviously, when the first peak increased, this second peak decreased because the remaining unpolymerized resin decreased. In this case, G and GoxNP showed

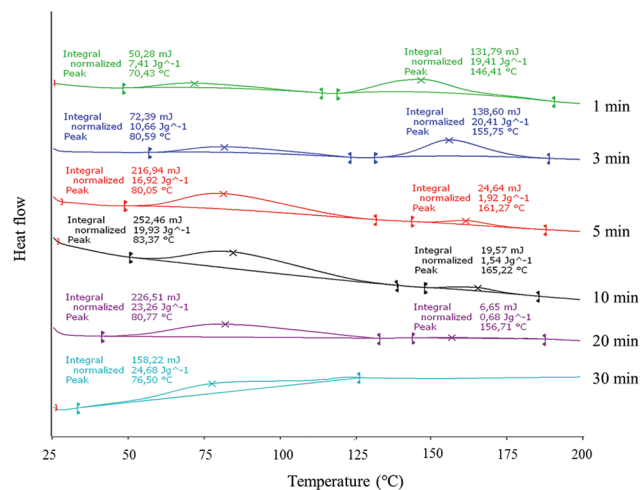


Figure 3. Differential scanning calorimetry thermograms of R as a function of different times of ultraviolet polymerization.

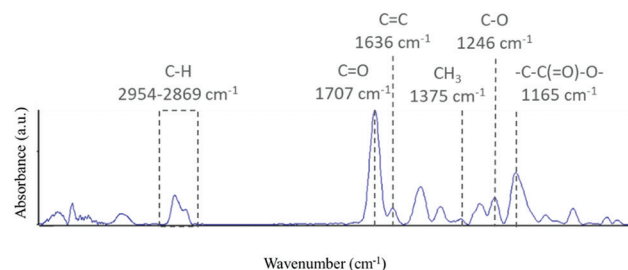


Figure 4. Fourier transform infrared spectra of uncured R.

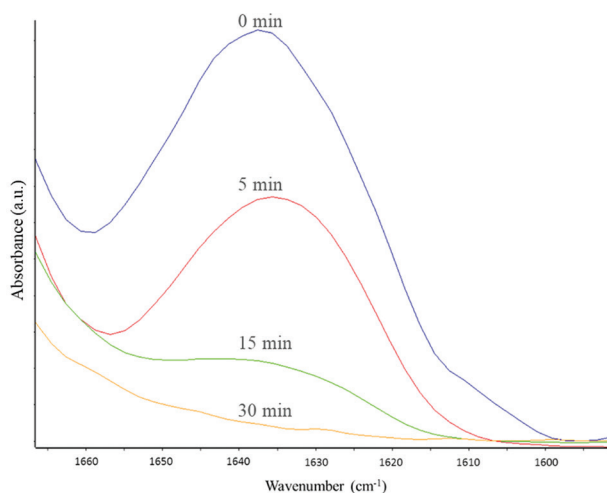


Figure 5. Fourier transform infrared spectra of C=C peak (1637 cm^{-1}) of R with different times of ultraviolet exposure.

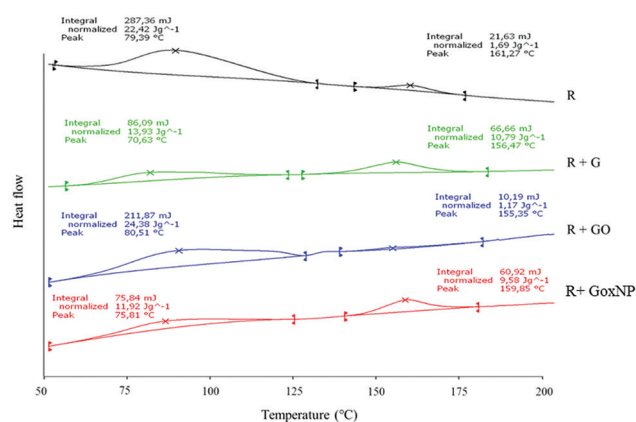


Figure 6. Differential scanning calorimetry thermograms of R, R+G, R+GO, R+GoxNP after 5 min of ultraviolet cure.

higher peaks than R and R+GO, confirming the lower UV polymerization degree.

When FTIR spectra were compared, the same tendency was observed. By studying the C=C peak at 1637 cm^{-1} (Figure 7), it is possible to compare the polymerization degree, which is more advanced when the peak is less intense.

The FTIR results showed that R+G and R+GoxNP followed the same trend when compared to the observed DSC data. After 5 min of UV exposure, their polymerization degree was lower than in the case of the pristine resin and R+GO.

Figure 8 showed the polymerization degree due to the UV exposure (Eq. 3.1) and data presented in Table 3, at different exposure times. It can be seen how GO retarded the polymerization process for short UV times; however, from 5 min of UV exposure, the polymerization degree was similar to R.

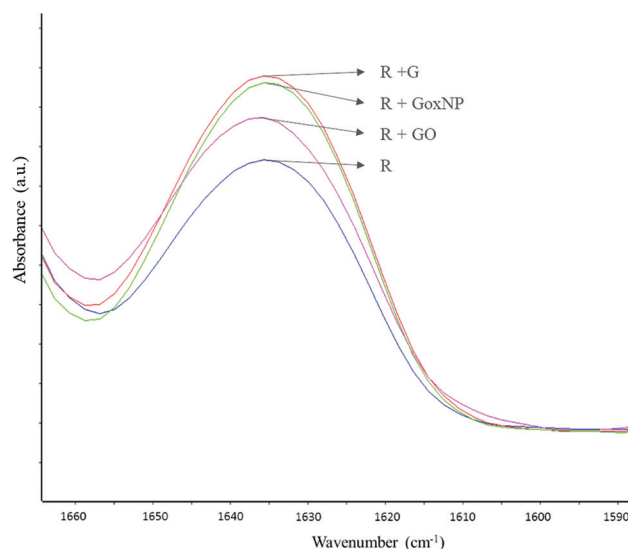


Figure 7. Fourier transform infrared spectra of C=C peak (1637 cm^{-1}) of R, R+G, R+GO, R+GoxNP after 5 min of ultraviolet cure.

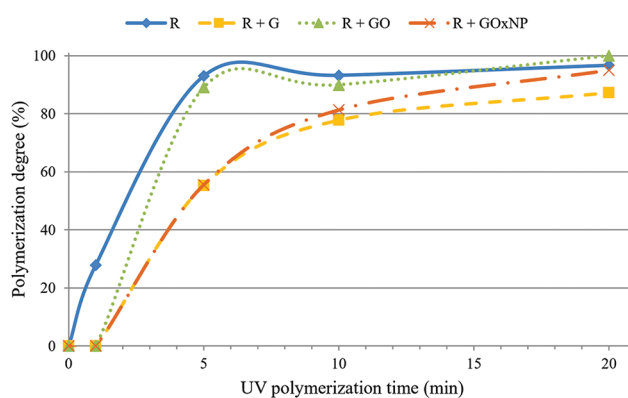


Figure 8. Polymerization degree versus ultraviolet polymerization time of R, R+G, R+GO, R+GoxNP.

On the other hand, R+G and R+GoxNP showed similar tendencies regarding the evolution of polymerization degree with time. The presence of these nanofillers showed a higher impact on the degree of polymerization when compared to GO, especially for relatively medium and long periods. They affect the process, achieving lower polymerization degrees than the initial resin; this effect was especially notable in the case of G.

Table 4 shows changes in hardness as a function of UV polymerization time for the different nanocomposites. In all cases, hardness increased with time, showing that the polymerization process was advancing. The trend observed in the hardness was similar to the obtained data from the DSC and FTIR analysis that the addition of G and GoxNP influenced the polymerization process of the resin; they did not allow the resin to cure completely.

Therefore, Shore D hardness was lower for these GBN. Whilst hardness value of R was 82 after 60 min of exposure time, R+G and R+GoxNP were 67 and 71, respectively. However, GO did not change the polymerization degree of resin – with a Shore D hardness of 81 after 60 min.

4.4. UV-visible spectroscopy

To determine if the presence of the nanofillers affects the UV absorption, the absorbance of the different uncured samples was measured by means of UV-visible spectroscopy. Wavelength was set at 405 nm, which was the same wavelength used by the printer. Results are shown in **Table 5**.

R was used as a reference and absorbance values showed the difference between the light absorption of R and the resin with the different nanofillers. In general, it was observed that in all cases, samples with nanofillers had higher absorbance than R, being especially noticeable in the case of R+G. These results suggest that G and GoxNP nanoparticles could be absorbing a significant part of the UV-light that reaches the sample.

4.5. Printability

Cube samples were printed with the different resins prepared as previously explained. An example of the resultant samples is shown in **Figure 9**.

It can be observed that R+GO and R+GoxNP samples showed good printability, whilst R+G presented important problems during printing process.

As R+GO showed similar polymerization degree than R, this mixture presented good printability. In the case of R+GoxNP, it seems that the slight decrease in polymerization degree showed did not impede structure formation by 3D printing. However, the effect of G on the UV polymerization of the resin prevented the

Table 4. Hardness of R, R+G, R+GO, R+GoxNP with different UV polymerization time

	R	R+G	R+GO	R+GoxNP
5 min	71 ± 1 ^a	43 ± 2 ^b	76 ± 2 ^a	53 ± 4 ^c
10 min	79 ± 1 ^a	54 ± 3 ^b	79 ± 2 ^a	65 ± 2 ^c
20 min	81 ± 1 ^a	63 ± 3 ^b	79 ± 2 ^a	69 ± 2 ^c
60 min	82 ± 2 ^a	67 ± 1 ^b	81 ± 1 ^a	71 ± 2 ^b

Values with different letters are significantly different ($P < 0.05$). Different mixtures for the same UV time (rows) were compared by ANOVA analysis, but different times (columns) were not compared between them.

Table 5. Absorbance at wavelength of 405 nm measured by UV-visible spectroscopy

	Absorbance at 405 nm (a.u.)
R+G	1.43
R+GO	0.32
R+GoxNP	1.10

structure to be properly formed. This could be due to a decrease in curing depth, leading to a lack of adhesion between layers when G is present. It could be related with the retardation in the UV polymerization previously discussed.

(1) Dimensional stability

Tables 6 and 7 show dimensional stability of the different samples. R+G samples are not included in this analysis because the printed samples did not demonstrate sufficient quality. Difference images – designed geometry versus printed geometry – were obtained by subtracting the reference image (CAD file) to the binary image, and these images were used to determine the percentage printing accuracy.

Comparing both geometries, it was found that in all cases, the accuracy for square-shaped geometry was higher than the circular-shaped geometry. Besides, it was noticed that in comparison with pristine resin, GO reduced slightly printing accuracy, whilst this parameter was not affected by GoxNP.

4.6. Dispersibility

Images taken to the captured from different surfaces are shown in **Figure 10**. It can be observed that the best dispersion is obtained for the sample R+GoxNP. In the case of R+GO, some agglomerates can be observed and more and larger agglomerates can be observed in R+G sample.

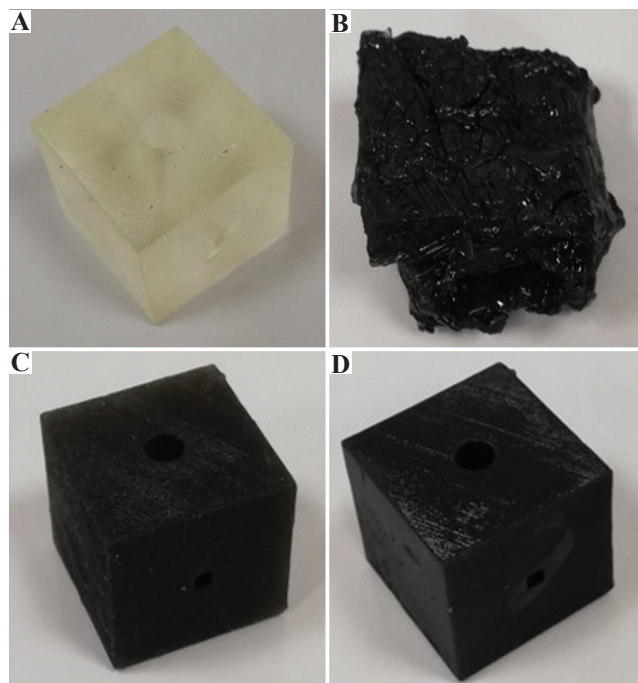


Figure 9. Printed cubes with R (A), R+G (B), R+GO (C) and R+GoxNP (D).

Table 6. Accuracy of printed samples with circular holes

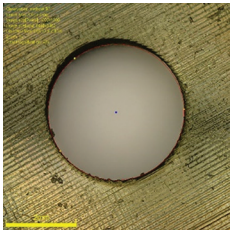
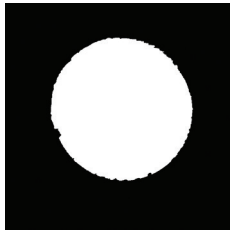
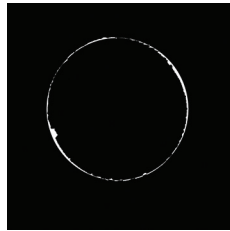
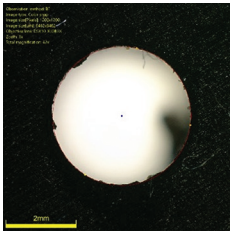
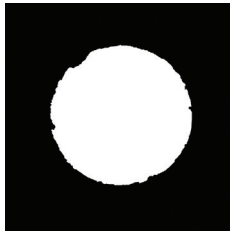
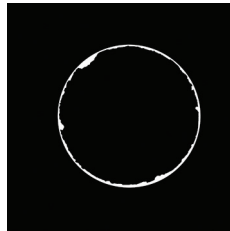
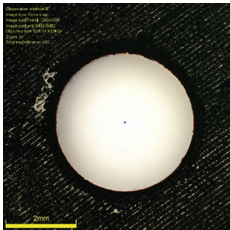
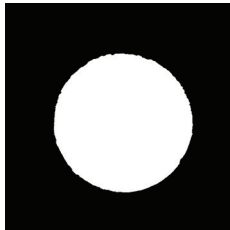
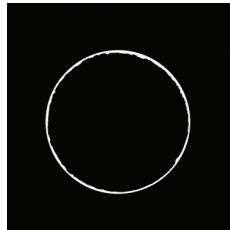
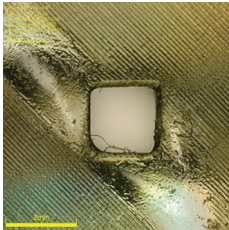
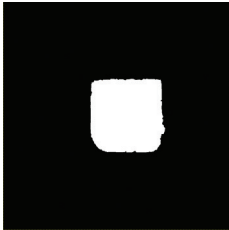
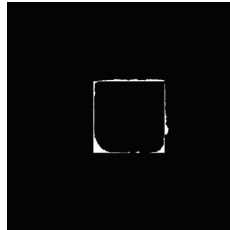
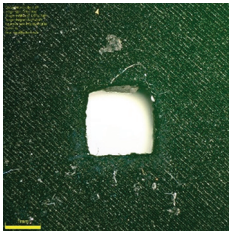
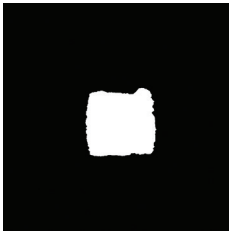
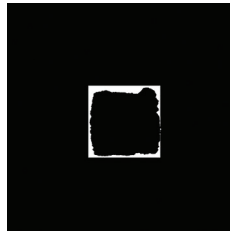

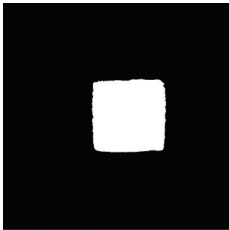
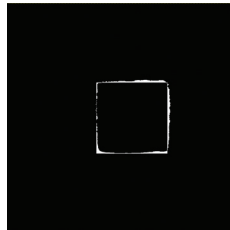
Sample	Original image	Binary image	Difference image	% Accuracy
R				98.61 ± 1.12
R+GO				96.92 ± 2.53
R+GoxNP				98.64 ± 0.14

Table 7. Accuracy of printed samples with square holes

Material type	Original image	Binary image	Difference image	% Accuracy
R				99.09 ± 0.31
R+GO				97.92 ± 0.50
R+GoxNP				99.11 ± 0.31

4.7. Thermal conductivity

Thermal conductivity measurements were completed to evaluate, together with viscosity, the nanofiller dispersion. Thermal conductivity decreases with free volume; therefore, it is possible to have information about it through thermal conductivity measurements.

Figure 11 shows the results obtained for different nanofillers. The addition of GoxNP slightly increased thermal conductivity, whilst G reduced this parameter. In the case of GO, thermal conductivity was not affected by this nanoparticle. However, differences found between the nanocomposites and R were not significant ($P > 0.05$).

4.8. Wettability

Water contact angle on the different investigated surfaces is presented in Table 8. These measurements could give

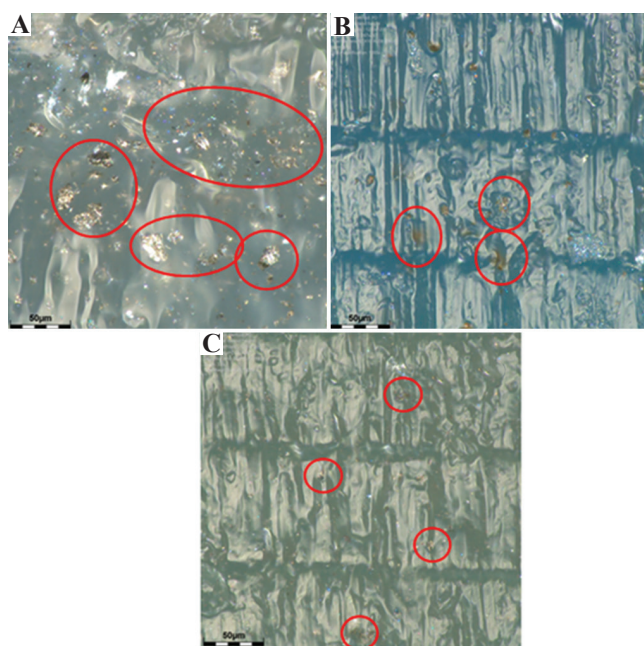


Figure 10. GBN dispersion of R+G (A), R+GO (B) and R+GoxNP (C). Red circles show graphene-based nanomaterials agglomerates of different size.

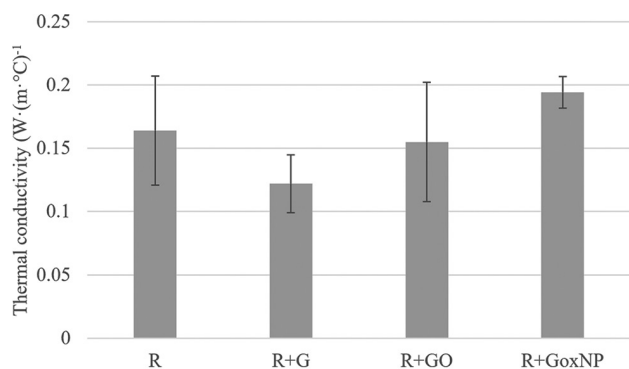


Figure 11. Thermal conductivity of R, R+G, R+GO, R+GoxNP.

information about layers adhesion, which could be related to printability.

R+GO and R+GoxNP slightly increased hydrophilicity of the resin. There were minor decreases in contact angle: 4% for R+GO and 6.2% for R+GoxNP. However, R+G showed a subtle increase in contact angle, which means that its hydrophilicity was lower. However, with the deviations that these values presented, differences were not significant.

4.9. Roughness

The R_a parameters of roughness of the different samples are shown in Table 9.

Roughness results showed that the addition of nanofillers may affect the roughness of 3D printed samples. These differences of surface roughness are due to the surface finish; the higher the roughness, the worse the surface finish. Therefore, these measurements were used as an indicator of the printing quality. Although there were no major differences, it could be observed that the addition of GoxNP did not affect roughness compared to R, GO addition slightly increased roughness (17%) and G showed the highest increase in roughness (34%).

5. Discussion

This study demonstrated the effect of different GBN on the polymerization reaction and the printability of an acrylic photocurable resin. It was found that G affected polymerization degree due to its high light absorption and therefore, it also affected printability. Conversely, GoxNP did affect polymerization degree slightly, but it allowed printing process. Finally, GO did not affect polymerization reaction nor printability of the resin. Although the differences on UV polymerization and wettability between G and GoxNP are subtle, their impact on the printing performance is highly notable due to the differences in light absorbance. R+G showed the highest light absorbance (Table 5). Therefore, G absorbs more light (1.43 a.u.) than GoxNP (1.10 a.u.) and curing depth could be reduced, leading to lower adhesion between layers and worse printability.

Polymerization reaction was studied using DSC, FTIR and hardness measurements. First, thermal polymerization was studied to investigate the effect of

Table 8. Contact angle (°) of water on sample surface

R	R+G	R+GO	R+GoxNP
72.9 ± 1.6	74.0 ± 3.7	70.0 ± 2.7	68.4 ± 3.6

Table 9. Roughness (R_a) of printed samples (µm)

R	R+G	R+GO	R+GoxNP
1.90 ± 0.24	2.56 ± 1.20	2.23 ± 0.53	1.87 ± 0.48

GBN on the polymerization separately from the effect on UV absorption. Hence, it was studied to find out if nanofillers influence the polymerization reaction by avoiding the polymer chain growth or terminating the polymerization process. The obtained results suggested that the incorporation of nanofillers did not influence the thermal polymerization process. Some studies^[46,47] explored the capability of G to act as free radical scavengers, which, in this study, could result in the capture of free radicals formed during polymerization leading to a slowdown of this process. However, in this study, GBN did not impede polymerization reaction acting as free radical scavengers.

In terms of UV polymerization, the results of this study have demonstrated that the incorporation of GBN has a significant impact on UV polymerization since the presence of these nanoparticles could affect the UV-visible light absorption. This effect could decrease the energy caught by the photoinitiator resulting in a lower polymerization degree. It was more noticeable with the addition of G than GO and GoxNP, which could be attributed to the darker color of G nanoparticles^[58]. The higher is the light absorption, the lower is the polymerization degree because the light that actually reaches the photoinitiator is reduced. G, GO and GoxNP showed different color, and therefore, they hamper the light absorption of the photoinitiator in different extents. G was the darkest, followed by GoxNP and finally, GO with a brownish color. All of them presented a decrease in polymerization degree at low exposure times; however, for high exposures times (> 5 min), G only achieved 87.3% compared to 96.7% in pristine resin. Conversely, GoxNP achieved a 95% and GO was similar to pristine resin. It was found that GBN does not change polymerization energy when this process is conducted by heating. For this reason, it seems that GBN does not affect polymerization energy when light is not involved in the process. Therefore, GBN avoid light to reach the photoinitiator and this is why differences in polymerization degree appeared.

The extent of the polymerization reaction determined the printability of the samples. If polymerization degree is not adequate, curing depth decreases, leading to lack of adhesion between layers. GO and GoxNP allowed the printing process with the same parameters than pristine resin, whilst G did not allow to obtain satisfactory printed structures. This negative effect on the printability suggests that the G resin did not present enough polymerization degree to achieve the minimum adhesion between layers to obtain a printed structure.

In terms of printing accuracy, GoxNP showed higher accuracy than GO and similar to R. Besides, the study of surface roughness revealed that the smoothest surface was obtained with R+GoxNP and it was similar

to R. These differences in accuracy could be explained by GBN dispersion. Viscosity results suggested that the dispersibility of GoxNP was slightly better than GO. Perhaps, the presence of agglomerates could diffract the light affecting to the accuracy of the printed cross-section. To the best of our knowledge, this effect has not been previously reported; however, some studies^[59] using other 3D printing technologies found that functionalized G nanoplatelets did not affect printing accuracy, except when the layer thickness was large. Besides, this study shows the good accuracy of SLA compared to other 3D printing techniques. For example, Zhou *et al.*^[51] found a maximum accuracy of 85.68% using powder-based ink-jet 3D printing.

Our results suggest that there was a relation between printability, dimensional stability and roughness. It was observed that the greater the effect of GBN on printability and dimensional stability, the higher the surface roughness. R+G showed the worst printability and printing accuracy and it presented the highest values of roughness, followed by R+GO. R+GoxNP had similar roughness and printing accuracy than R.

In relation to nanoparticle dispersion, the differences observed between G, GO and GoxNP could be better understood from a chemical point of view. Both GO and GoxNP had oxygenated groups in their composition. These groups were responsible for the better interaction between the nanomaterial and the matrix thanks to the polarity of the nanomaterial, which increases the stability of the dispersion^[60]. It was seen in viscosity, glass transition temperature, and thermal conductivity measurements.

It has been reported that an increase in viscosity is expected when nanofillers are well-dispersed since more surface area is available for interaction with the matrix^[61]. Therefore, an increase of GO and GoxNP viscosity could suggest a homogenous dispersion of the nanofiller, which is probably improved due to the presence of the oxygenated groups on their surface. Conversely, the addition of G decreased the viscosity, suggesting a poor dispersion of these nanoparticles within the polymer matrix. Similar findings were reported in other studies^[54,62,63].

This decrease in the viscosity caused by the nanoparticles addition was attributed to some physicochemical phenomena. Jain *et al.*^[62] postulated that the decrease in viscosity could be due to a selective physisorption of the highest molecular weight polymer chains on the nanoparticle surface, leaving low molar mass in the surrounding molten matrix. Conversely, Merkel *et al.*^[54] explained the decrease in viscosity by the excluded free volume induced around the nanoparticles, which was accompanied by a reduction in the T_g .

Therefore, since a decrease in T_g of G samples was found, it could be concluded that the addition of G

probably led to a decrease in viscosity due to the excluded free volume induced around the nanoparticles. In the case of GO and GoxNP, viscosity was higher than R because their dispersion was homogeneous and no changes were found in T_g .

In any case, despite the increase in viscosity observed when some nanofillers were added, the viscosity is adequate for 3D printing since the values measured are ≤ 5 Pa·s, which is the highest viscosity recommended^[39].

The study of thermal conductivity led to a similar conclusion: the slight decrease in thermal conductivity of R+G samples was due to the excluded free volume induced as a result of the presence of agglomerates.

In general, the larger particle size of the nanofillers improves the exfoliation degree, dispersion of nanoparticles and interfacial connections with the matrix, thereby enhancing the thermal conductivity^[64]. Furthermore, it is known that thermal conductivity increases when the average size increases and the number of layers decreases due to the smaller total thermal boundary resistances from the interface area^[65]. The higher thermal conductivity of R+GoxNP could be explained by its size and dispersion. According to data sheet, GoxNP average size (200-300 nm) is 100 times the average size of GO (1.8 – 2.7 nm). Besides, viscosity measurements show better dispersion of GoxNP than G and GO.

In the case of G, a reduction of thermal conductivity was observed. It could be due to the poor dispersion of G within the matrix and the increase in excluded free volume, which could corroborate the viscosity results and its effect on printability.

Previous studies^[66] found that adding 0.5 wt% of GO to an epoxy resin leads to an increase in thermal conductivity of more than 200%. However, another study^[67] found that GO presented no effect on thermal conductivity of epoxy resin until a load of 2 wt% was added. Conversely, Wang *et al.*^[68] studied the effect of graphene nanoplatelets on thermal conductivity by adding 25 vol%.

Therefore, the effect of nanofillers on thermal conductivity depends on many factors, such as the degree of dispersion. In this case, no significant effect was found, and it could be due to the low amount added. If a larger amount of well-dispersed GBN were added, free volume would be reduced and thermal conductivity would increase^[69].

Finally, wettability was studied. Previous studies have investigated the effect of GBN addition on the hydrophilicity of polymers. It was found that the addition of GO coating to PCL scaffolds increased hydrophilicity^[40]. Different oxidation degrees was also studied and it was concluded that the higher the O/C ratio of G, the higher the hydrophilicity^[70,71].

In this study, it is noted that both GO and GoxNP increased slightly the wettability of the resin, which could be due to their hydrophilic oxygenated groups (carboxyl, hydroxyl and epoxide functional groups)^[72]. In contrast, the contact angle of R+G is subtly higher than R, which could be due to the lack of oxygenated groups present on the G surface. However, there are no significant differences between R and R+G; hence, printability issues do not seem to be caused by wetting problems between liquid and cured resin.

In general, wettability is defined by surface energy; however, roughness can affect it. The results of this study do not show a relation between roughness and wettability. Therefore, it could be concluded that in this case, wettability was affected mainly by chemical functional groups and it was not related with roughness.

Our results show a first approach to understand the effect of GBN on resin polymerization. The current study attempted to simulate the printing process by exposing the resin to UV light followed by DSC analysis. However, the designed methodology differs in the polymerization of resin during printing process because of the light source – 3D printer uses a punctual laser light and Form Cure uses a UV lamp. Therefore, the effect of other parameters, such as the UV source power or intensity, should be studied. Besides, different techniques to improve dispersion (e.g., combination of mechanical stirring and sonication) should be tested.

It has been proven that the GBN is viable to be used as fillers of photocurable resins; for potential applications, continued investigations on these nanocomposites are necessary. For example, it would be interesting to test them mechanically to assure their suitability to build 3D-printed structures with improved properties, and cell studies should be carried out to assure the effect of GBN in cell adhesion, proliferation and differentiation.

6. Conclusions

Before using a nanocomposite to print structures, it is important to discern the effect that nanofillers will have on the whole printing process, since it has been observed that the dispersion of nanofillers on SLA resin can compromise many parameters, ranging from viscosity of the blended resin to printability properties.

Despite the negative effect that GoxNP showed on polymerization degree, it has been proven that the incorporation of 0.1 wt% of GO and GoxNP to the photocured resin did not significantly affect printing quality, allowing their use in the preparation of new nanofilled photocurable resins for SLA printing. However, it has been observed that the addition of 0.1 wt% G demonstrated a notable negative effect on the printability. This could be explained by the differences in type, functionalization and structure of GBN that change

dispersibility and light absorbance. Nevertheless, negative effect of G is not an indication that it is not possible to print with R+G mixture but printing parameters must be optimized to compensate the negative effect of G on polymerization.

Therefore, understanding how GBN affects polymerization and the properties of the resin is crucial to adapt printing parameters (e.g., light intensity, exposure time, layer thickness, etc.) and resin formulation (e.g., maximum permissible nanoparticles amount, photoinitiator amount, etc.) to improve 3D printing that capitalizes on SLA accuracy.

Acknowledgments

We would like to thank to Mariano Jiménez.

Funding

This work was supported by Comillas Pontifical University (grant number PP2020_08).

Conflict of interest

No conflict of interest was reported by all authors.

Author contributions

S.F., Y.B. and E.P. conceptualization. S.L., S.F. and E.P. data collection. S.L., Y.B. and J.C.D.R. analysis and interpretation of results. S.L. and E.P. writing, original draft preparation. S.F., Y.B., J.C.D.R. and N.D. writing, review and editing. J.C.D.R., N.D. and E.P. supervision. All authors reviewed the results and approved the final version of the manuscript.

References

- Borrello J, Nasser P, Iatridis JC, *et al.*, 2018, 3D Printing a Mechanically-Tunable Acrylate Resin on a Commercial DLP-SLA Printer. *Addit Manuf*, 23:374–80. <https://doi.org/10.1016/j.addma.2018.08.019>
- Borrello J, Backeris P, 2017, Rapid Prototyping Technologies. In: *Rapid Prototyping in Cardiac Disease: 3D Printing the Heart*, p41–9. https://doi.org/10.1007/978-3-319-53523-4_5
- Vasamsetty P, Pss T, Kukkala D, *et al.*, 2020, 3D Printing in Dentistry-Exploring the New Horizons. *Mater Today*, 26:838–41. <https://doi.org/10.1016/j.matpr.2020.01.049>
- Baumgartner S, Gmeiner R, Schönherr JA, *et al.*, 2020, Stereolithography-Based Additive Manufacturing of Lithium Disilicate Glass Ceramic for Dental Applications. *Mater Sci Eng C*, 116:111180. <https://doi.org/10.1016/j.msec.2020.111180>
- Schüller-Ravoo S, Teixeira SM, Feijen J, *et al.*, 2013, Flexible and Elastic Scaffolds for Cartilage Tissue Engineering Prepared by Stereolithography Using Poly (Trimethylene Carbonate)-Based Resins. *Macromol Biosci*, 13:1711–9. <https://doi.org/10.1002/mabi.201300399>
- Sodian R, Loebe M, Hein A, *et al.*, 2002, Application of Stereolithography for Scaffold Fabrication for Tissue Engineered Heart Valves. *ASAIO J*, 48:12–6. <https://doi.org/10.1097/00002480-200201000-00004>
- Lee KW, Wang S, Fox BC, *et al.*, 2007, Poly (Propylene Fumarate) Bone Tissue Engineering Scaffold Fabrication using Stereolithography: Effects of Resin Formulations and Laser Parameters. *Biomacromolecules*, 8:1077–84. <https://doi.org/10.1021/bm060834v>
- Lu F, Wu R, Shen M, *et al.*, 2021, Rational Design of Bioceramic Scaffolds with Tuning Pore Geometry by Stereolithography: Microstructure Evaluation and Mechanical Evolution. *J Eur Ceram Soc*, 41:1672–82. <https://doi.org/10.1016/j.jeurceramsoc.2020.10.002>
- Dabbagh SR, Sarabi MR, Rahbarghazi R, *et al.*, 2020, 3D-Printed Microneedles in Biomedical Applications. *iScience*, 24:102012. <https://doi.org/10.1016/j.isci.2020.102012>
- Xenikakis I, Tzimtzimis M, Tsongas K, *et al.*, 2019, Fabrication and Finite Element Analysis of Stereolithographic 3D Printed Microneedles for Transdermal Delivery of Model Dyes Across Human Skin *In Vitro*. *Eur J Pharm Sci*, 137:104976. <https://doi.org/10.1016/j.ejps.2019.104976>
- Wang J, Goyanes A, Gaisford S, *et al.*, 2016, Stereolithographic (SLA) 3D Printing of Oral Modified-Release Dosage Forms. *Int J Pharm*, 503:207–212. <https://doi.org/10.1016/j.ijpharm.2016.03.016>
- Karakurt I, Aydoğdu A, Çıkrıkçı S, *et al.*, 2020, Stereolithography (SLA) 3D Printing of Ascorbic acid Loaded Hydrogels: A Controlled Release Study. *Int J Pharm*, 584:119482. <https://doi.org/10.1016/j.ijpharm.2020.119428>
- Chen X, Ware HO, Baker E, *et al.*, 2017, The Development of an All-polymer-based Piezoelectric Photocurable Resin for Additive Manufacturing. *Procedia CIRP*, 65:157–62. <https://doi.org/10.1016/j.procir.2017.04.025>
- Cheng WT, Chih YW, Yeh WT, 2007, *In Situ* Fabrication of Photocurable Conductive Adhesives with Silver Nanoparticles in the Absence of Capping Agent. *Int J Adhes Adhes*, 27:236–43.

- <https://doi.org/10.1016/j.ijadhadh.2006.05.001>
15. Sciancalepore C, Moroni F, Messori M, et al., 2017, Acrylate-Based Silver Nanocomposite by Simultaneous Polymerization-Reduction Approach via 3D Stereolithography. *Compos Commun*, 6:11–6.
<https://doi.org/10.1016/j.coco.2017.07.006>
 16. Scordo G, Bertana V, Scaltrito L, et al., 2019, A Novel Highly Electrically Conductive Composite Resin for Stereolithography. *Mater Today Commun*, 19:12–7.
<https://doi.org/10.1016/j.mtcomm.2018.12.017>
 17. Mu Q, Wang L, Dunn CK, et al., 2017 Digital Light Processing 3D Printing of Conductive Complex Structures. *Addit Manuf*, 18:74–83.
<https://doi.org/10.1016/j.addma.2017.08.011>
 18. Szaloki M, Gall J, Bukovinszki K, et al., 2013, Synthesis and Characterization of Cross-Linked Polymeric Nanoparticles and their Composites for Reinforcement of Photocurable Dental Resin. *React Funct Polym*, 73:465–73.
<https://doi.org/10.1016/J.REACTFUNCTPOLYM.2012.11.013>
 19. dos Santos MN, Opelt CV, Lafratta FH, et al., 2011, Thermal and Mechanical Properties of a Nanocomposite of a Photocurable Epoxy-Acrylate Resin and Multiwalled Carbon Nanotubes. *Mater Sci Eng A*, 528:4318–24.
<https://doi.org/10.1016/j.msea.2011.02.036>
 20. Zhang J, Huang D, Liu S, et al., 2019, Zirconia Toughened Hydroxyapatite Biocomposite Formed by a DLP 3D Printing Process for Potential Bone Tissue Engineering. *Mater Sci Eng C*, 105:110054.
<https://doi.org/10.1016/j.msec.2019.110054>
 21. Markandan K, Lai CQ, 2020, Enhanced Mechanical Properties of 3D Printed Graphene-Polymer Composite Lattices at Very Low Graphene Concentrations. *Compos A Appl Sci Manuf*, 129:105726.
<https://doi.org/10.1016/j.compositesa.2019.105726>
 22. Zhou X, Nowicki M, Cui H, et al., 2017, 3D Bioprinted Graphene Oxide-Incorporated Matrix for Promoting Chondrogenic Differentiation of Human Bone Marrow Mesenchymal Stem Cells. *Carbon*, 116:615–24.
<https://doi.org/10.1016/j.carbon.2017.02.049>
 23. Chung CM, Kim JG, Kim MS, et al., 2002, Development of a New Photocurable Composite Resin with Reduced Curing Shrinkage. *Dent Mater*, 18:174–8.
[https://doi.org/10.1016/S0109-5641\(01\)00039-2](https://doi.org/10.1016/S0109-5641(01)00039-2)
 24. Iqbal AA, Sakib N, Iqbal AP, et al., 2020, Graphene-Based Nanocomposites and their Fabrication, Mechanical Properties and Applications. *Materialia*, 12:100815.
<https://doi.org/10.1016/j.mtla.2020.100815>
 25. Azizi-Lalabadi M, Jafari SM, 2021, Bio-Nanocomposites of Graphene with Biopolymers; Fabrication, Properties, and Applications. *Adv Coll Interface Sci*, 292:102416.
<https://doi.org/10.1016/j.cis.2021.102416>
 26. Li Y, Feng Z, Huang L, et al., 2019, Additive Manufacturing High Performance Graphene-Based Composites: A Review. *Compos A Appl Sci Manuf*, 124:105483.
<https://doi.org/10.1016/j.compositesa.2019.105483>
 27. Guo S, Lu Y, Wan X, et al., 2020, Preparation, Characterization of Highly Dispersed Reduced Graphene Oxide/Epoxy Resin and Its Application in Alkali-Activated Slag Composites. *Cem Concr Compos*, 105:103424.
<https://doi.org/10.1016/j.cemconcomp.2019.103424>
 28. Pour ZS, Ghaemy M, 2016, Polymer Grafted Graphene Oxide: For Improved Dispersion in Epoxy Resin and Enhancement of Mechanical Properties of Nanocomposite. *Compos Sci Technol*, 136:145–57.
<https://doi.org/10.1016/j.compscitech.2016.10.014>
 29. Al-Asadi AS, Hassan QM, Abdulkader AF, et al., 2019, Formation of Graphene Nanosheets/Epoxy Resin Composite and Study Its Structural, Morphological and Nonlinear Optical Properties. *Opt Mater*, 89:460–467.
<https://doi.org/10.1016/j.optmat.2019.01.078>
 30. Kilic U, Sherif MM, Ozbulut OE, 2019, Tensile Properties of Graphene Nanoplatelets/Epoxy Composites Fabricated by Various Dispersion Techniques. *Polym Test*, 76:181–91.
<https://doi.org/10.1016/j.polymertesting.2019.03.028>
 31. Wang X, Tang F, Qi X, et al., 2019, Mechanical, Electrochemical, and Durability Behavior of Graphene Nano-Platelet Loaded Epoxy-Resin Composite Coatings. *Compos B Eng*, 176:107103.
<https://doi.org/10.1016/j.compositesb.2019.107103>
 32. Sánchez-Hidalgo R, Yuste-Sánchez V, Verdejo R, et al., 2018, Main Structural Features of Graphene Materials Controlling the Transport Properties of Epoxy Resin-Based Composites. *Eur Polym J*, 101:56–65.
<https://doi.org/10.1016/j.eurpolymj.2018.02.018>
 33. Moriche R, Prolongo SG, Sánchez M, et al., 2015, Morphological Changes on Graphene Nanoplatelets Induced during Dispersion into an Epoxy Resin by Different Methods. *Compos B Eng*, 72:199–205.
<https://doi.org/10.1016/j.compositesb.2014.12.012>
 34. Fang F, Ran S, Fang Z, et al., 2019, Improved Flame Resistance and Thermo-Mechanical Properties of Epoxy Resin Nanocomposites from Functionalized Graphene Oxide Via Self-Assembly in Water. *Compos B Eng*, 165:406–16.
<https://doi.org/10.1016/j.compositesb.2019.01.086>

35. Kugler S, Kowalczyk K, Spychaj T, 2015, Hybrid Carbon Nanotubes/Graphene Modified Acrylic Coats. *Progress Org Coat*, 85:1–7.
<https://doi.org/10.1016/j.porgcoat.2015.02.019>
36. Baig Z, Mamat O, Mustapha M, *et al.*, 2018, Investigation of Tip Sonication Effects on Structural Quality of Graphene Nanoplatelets (GNPs) for Superior Solvent Dispersion. *Ultrason Sonochem*, 45:133–49.
<https://doi.org/10.1016/j.ultsonch.2018.03.007>
37. Lin D, Jin S, Zhang F, *et al.*, 2015, 3D Stereolithography Printing of Graphene Oxide Reinforced Complex Architectures. *Nanotechnology*, 26:434003.
<https://doi.org/10.1088/0957-4484/26/43/434003>
38. Feng Z, Li Y, Hao L, *et al.*, 2019, Graphene-Reinforced Biodegradable Resin Composites for Stereolithographic 3D Printing of Bone Structure Scaffolds. *J Nanomater*, 2019:1–13.
<https://doi.org/10.1155/2019/9710264>
39. Manapat JZ, Mangadlao JD, Tiu BD, *et al.*, 2017, High-Strength Stereolithographic 3D Printed Nanocomposites: Graphene Oxide Metastability. *ACS Appl Mater Interface*, 9:10085–93.
<https://doi.org/10.1021/acsami.6b16174>
40. Lipovka A, Rodriguez R, Bolbasov E, *et al.*, 2020, Time-Stable Wetting Effect of Plasma-Treated Biodegradable Scaffolds Functionalized with Graphene Oxide. *Surf Coat Technol*, 388:125560.
<https://doi.org/10.1016/j.surfcoat.2020.125560>
41. Lim SM, Shin BS, Kim K, 2017, Characterization of Products Using Additive Manufacturing with Graphene/Photopolymer-Resin Nano-Fluid. *J Nanosci Nanotechnol*, 17:5492–55.
<https://doi.org/10.1166/jnn.2017.14159>
42. Moriche R, Artigas J, Reigosa L, *et al.*, 2019, Modifications Induced in Photocuring of Bis-GMA/TEGDMA by the Addition of Graphene Nanoplatelets for 3D Printable Electrically Conductive Nanocomposites. *Compos Sci Technol*, 184:107876.
<https://doi.org/10.1016/j.compscitech.2019.107876>
43. Weng Z, Zhou Y, Lin W, *et al.*, 2016, Structure-Property Relationship of Nano Enhanced Stereolithography Resin for Desktop SLA 3D Printer. *Compos A Appl Sci Manuf*, 88:234–42.
<https://doi.org/10.1016/j.compositesa.2016.05.035>
44. Paz E, Ballesteros Y, Abenojar J, *et al.*, 2019, Graphene Oxide and Graphene Reinforced PMMA Bone Cements: Evaluation of Thermal Properties and Biocompatibility. *Materials*, 12:3146.
<https://doi.org/10.3390/ma12193146>
45. Abenojar J, Del Real JC, Ballesteros Y, *et al.*, 2018, Kinetics of Curing Process in Carbon/Epoxy Nano-Composites. *IOP Conf Ser Mater Sci Eng*, 369:012011.
<https://doi.org/10.1088/1757-899X/369/1/012011>
46. Liang H, Bu Y, Zhang Y, *et al.*, 2015, Graphene Oxide as Efficient High-Concentration Formaldehyde Scavenger and Reutilization in Supercapacitor. *J Coll Interface Sci*, 444:109–14.
<https://doi.org/10.1016/j.jcis.2014.12.063>
47. Xia W, Xue H, Wang J, *et al.*, 2016, Functionized Graphene Serving as Free Radical Scavenger and Corrosion Protection in Gamma-Irradiated Epoxy Composites. *Carbon*, 101:315–23.
<https://doi.org/10.1016/j.carbon.2016.02.004>
48. Martin-Gallego M, Hernández M, Lorenzo V, *et al.*, 2012, Cationic Photocured Epoxy Nanocomposites Filled with Different Carbon Fillers. *Polymer*, 53:1831–8.
<https://doi.org/10.1016/j.polymer.2012.02.054>
49. Paz E, Forriol F, del Real JC, *et al.*, 2017, Graphene Oxide Versus Graphene for Optimisation of PMMA Bone Cement for Orthopaedic Applications. *Mater Sci Eng C*, 77:1003–11.
<https://doi.org/10.1016/j.msec.2017.03.269>
50. Courtecuisse F, Karasu F, Allonas X, *et al.*, 2016, Confocal Raman Microscopy Study of Several Factors Known to Influence the Oxygen Inhibition of Acrylate Photopolymerization Under LED. *Progress Org Coat*, 92:1–7.
<https://doi.org/10.1016/j.porgcoat.2015.11.020>
51. Zhou ZX, Buchanan F, Lennon A, *et al.*, 2014, Investigating Approaches for Three-Dimensional Printing of Hydroxyapatite Scaffolds for Bone Regeneration. *Key Eng Mater*, 631:306–11.
<https://doi.org/10.4028/www.scientific.net/kem.631.306>
52. Hakvoort G, van Reijen L, 1985, Measurement of the Thermal Conductivity of Solid Substances by DSC. *Thermochim Acta*, 93:317–20.
53. Sousa I, Mendes A, Pereira RF, *et al.*, 2014, Collagen Surface Modified Poly (ϵ -Caprolactone) Scaffolds with Improved Hydrophilicity and Cell Adhesion Properties. *Mater Lett*, 134:263–7.
<https://doi.org/10.1016/j.matlet.2014.06.132>
54. Merkel TC, Freeman BD, Spontak RJ, *et al.*, 2002, Ultraporous, Reverse-Selective Nanocomposite Membranes. *Science*, 296:519–22.
<https://doi.org/10.1126/science.1069580>
55. Vicard C, de Almeida O, Cantarel A, *et al.*, 2017, Experimental Study of Polymerization and Crystallization Kinetics of Polyamide 6 Obtained by Anionic Ring Opening Polymerization of ϵ -Caprolactam. *Polymer*, 132:88–97.

- <https://doi.org/10.1016/j.polymer.2017.10.039>
56. Tudorachi N, Bunia I. 2015, Synthesis and Thermal Investigation by TG-FTIR-MS Analysis of Some Functionalized Acrylic Copolymers and Magnetic Composites with Fe₃O₄. *J Anal Appl Pyrolysis*, 116:190–201. <https://doi.org/10.1016/j.jaap.2015.09.010>
 57. Ortiz-Herrero L, Cardaba I, Setien S, *et al.*, 2019, OPLS Multivariate Regression of FTIR-ATR Spectra of Acrylic Paints for Age Estimation in Contemporary Artworks. *Talanta*, 205:120114. <https://doi.org/10.1016/j.talanta.2019.120114>
 58. Chiappone A, Roppolo I, Naretto E, *et al.*, 2017, Study of Graphene Oxide-Based 3D Printable Composites: Effect of the *In Situ* Reduction. *Compos B Eng*, 124:9–15. <https://doi.org/10.1016/j.compositesb.2017.05.049>
 59. García E, Núñez PJ, Chacón JM, *et al.*, 2020, Comparative Study of Geometric Properties of Unreinforced PLA and PLA-Graphene Composite Materials Applied to Additive Manufacturing Using FFF Technology. *Polym Test*, 91:106860. <https://doi.org/10.1016/j.polymertesting.2020.106860>
 60. Chouhan A, Mungse HP, Khatri OP, 2020, Surface Chemistry of Graphene and Graphene Oxide: A Versatile Route for their Dispersion and Tribological Applications. *Adv Coll Interface Sci*, 283:102215. <https://doi.org/10.1016/j.cis.2020.102215>
 61. Miller SG, Bauer JL, Maryanski MJ, *et al.*, 2010, Characterization of Epoxy Functionalized Graphite Nanoparticles and the Physical Properties of Epoxy Matrix Nanocomposites. *Compos Sci Technol*, 70:1120–5. <https://doi.org/10.1016/j.compscitech.2010.02.023>
 62. Jain S, Goossens JG, Peters GW, *et al.*, 2008, Strong Decrease in Viscosity of Nanoparticle-Filled Polymer Melts through Selective Adsorption. *Soft Matter*, 4:1848–54. <https://doi.org/10.1039/b802905a>
 63. Mackay M., Dao T., Tuteja A, *et al.*, 2003, Nanoscale Effects Leading to Non-Einstein-Like Decrease in Viscosity. *Nat Mater*, 2:762–66.
 64. Rafiee M, Nitzsche F, Laliberte J, *et al.*, 2019, Thermal Properties of Doubly Reinforced Fiberglass/Epoxy Composites with Graphene Nanoplatelets, Graphene Oxide and Reduced-Graphene Oxide. *Compos B Eng*, 164:1–9. <https://doi.org/10.1016/j.compositesb.2018.11.051>
 65. Sun Y, Tang B, Huang W, *et al.*, 2016, Preparation of Graphene Modified Epoxy Resin with High Thermal Conductivity by Optimizing the Morphology of Filler. *Appl Therm Eng*, 103:892–900. <https://doi.org/10.1016/j.applthermaleng.2016.05.005>
 66. Aradhana R, Mohanty S, Nayak SK, 2018, Comparison of Mechanical, Electrical and Thermal Properties in Graphene Oxide and Reduced Graphene Oxide Filled Epoxy Nanocomposite Adhesives. *Polymer*, 141:109–23. <https://doi.org/10.1016/j.polymer.2018.03.005>
 67. Huang T, Zeng X, Yao Y, *et al.*, 2016, Boron nitride@graphene Oxide Hybrids for Epoxy Composites with Enhanced Thermal Conductivity. *RSC Adv*, 6:35847–54. <https://doi.org/10.1039/c5ra27315c>
 68. Wang J, Li JJ, Weng GJ, *et al.*, 2020, The Effects of Temperature and Alignment State of Nanofillers on the Thermal Conductivity of Both Metal and Nonmetal Based Graphene Nanocomposites. *Acta Mater*, 185:461–73. <https://doi.org/10.1016/j.actamat.2019.12.032>
 69. Xue G, Zhong J, Gao S, *et al.*, 2016, Correlation between the Free Volume and Thermal Conductivity of Porous Poly (Vinyl Alcohol)/Reduced Graphene Oxide Composites Studied by Positron Spectroscopy. *Carbon*, 96:871–8. <https://doi.org/10.1016/j.carbon.2015.10.041>
 70. Li J, Yu Y, Chen D, *et al.*, 2020, Hydrophilic Graphene Aerogel Anodes Enhance the Performance of Microbial Electrochemical Systems. *Bioresour Technol*, 304:122907. <https://doi.org/10.1016/j.biortech.2020.122907>
 71. Hou Y, Wang W, Bártolo P, 2020, Investigating the Effect of Carbon Nanomaterials Reinforcing Poly (ϵ -Caprolactone) Printed Scaffolds for Bone Repair Applications. *Int J Bioprint*, 6:1–9. <https://doi.org/10.18063/ijb.v6i2.266>
 72. Yang S, Sha S, Lu H, *et al.*, 2021, Graphene Oxide and Reduced Graphene Oxide Coated Cotton Fabrics with Opposite Wettability for Continuous Oil/Water Separation. *Sep Purif Technol*, 259:118095. <https://doi.org/10.1016/j.seppur.2020.118095>

Publisher's note

Whioce Publishing remains neutral with regard to jurisdictional claims in published maps and institutional affiliations.